Methodology for design of antialiasing filters for autostereoscopic displays

Atanas Boev, Robert Bregovic, Atanas Gotchev

Department of Signal Processing, Tampere University of Technology, Tampere, Finland

firstname.lastname@tut.fi

ABSTRACT

Multi-view autostereoscopic displays can be considered as a kind of a multirate system due to the construction compromise between the number of different views and spatial resolution adopted for such displays. Images to be visualized on these displays are prone to aliasing errors. Careful antialiasing requires knowledge about the display frequency response, which is determined mainly by the view sub-sampling topology but it is also influenced by some other, generally nonlinear, aliasing-causing display effects. In this work, a methodology for designing antialiasing filters for autostereoscopic displays is proposed. It includes the following three steps: 1) measuring aliasing effects by a set of test images – displayed on the screen, then photographed and then analyzed in Fourier domain; 2) estimating the display passband based on the set of measurements; and 3) designing filters confined to the so-estimated band. Using this methodology, one non-separable and three separable antialiasing filters have been designed. The non-separable filter cancels the aliasing terms completely, while the separable approximations allow for some small amount of aliasing for the sake of perceptually-favored sharpness preservation. The advantage of the methodology with respect to previously suggested antialiasing filter design approaches is demonstrated by objective comparisons of filter performance and computational efficiency and by visual inspection on a set of test images.

1. INTRODUCTION

In the recent years, a new group of 3D displays, referred to as *autostereoscopic displays*, has emerged. Such displays create illusion of depth by delivering separate images to each observer's eye without a need for special glasses. Instead, they operate by redirecting the light coming from pixels of a conventional TFT-LCD to different directions thus forming two or multiple views. The effect of redirecting the light is achieved by an optical filter, mounted on top of the LCD surface [1], [2], [3]. There are two common types of optical filters – lenticular sheet [1] which works by refracting the light, and parallax barrier [3] which works by blocking the light in certain directions.

Conventional TFT displays recreate full colour range by emitting light though red, green and blue coloured components (*sub-pixels*). In autostereoscopic mode, sub-pixels appear displaced in respect to the optical filter, and their light is redirected towards different positions. The effect is illustrated in Figure 1(a). The image, formed by the set of sub-pixels, visible from given direction is said to form a *view* [1], [2]. For each view, there is an *optimal observation spot*, where the view is perceived with maximum brightness. The range of angles from which a view can be seen, even though with diminished brightness, is known as the *visibility zone* of that view. Usually, the visibility zones of all views appear in horizontal direction in front of the display, as depicted in Figure 1(b). In order to visualize a scene in 3D, each view should represent different observation of that scene. The process of mapping an image to the sub-pixels corresponding to one view is called *view interleaving* [1], [4]. The map of correspondences between addressable sub-pixels of the display and the view they belong to is called *interleaving map*. Usually the interleaving map has repetitive

structure, which can be represented by an *interleaving pattern* copied multiple times over the display surface. In order to balance horizontal versus vertical resolution of each view, the optical filter is mounted at a slant to the TFT matrix. As a result, the sub-pixels visible from certain observation appear on a non-rectangular grid, which follows the slant of the optical filter. An example of such grid is given by the sub-pixels marked with "F" in Figure 2(a).

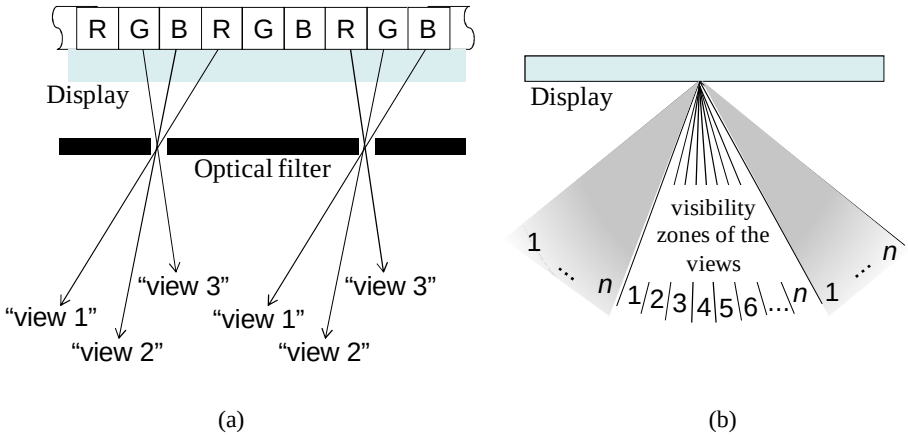

Figure 1, Operation principles of multi-view displays: a) Light redirection by optical filter, b) visibility zones

By moving laterally in front of a multi-view display, one can notice the discrete structure of the views seeing particular types of artefacts. One is *image flipping*, caused by the noticeable transition between the viewing zones, and the other is *picket fence effect*, caused by the gaps between sub-pixels being predominantly visible for some observation angles. The common practice to mitigate these effects is to broaden the visibility angle of each view, thus interspersing the visibility zones [1]. Thus, for any observation angle, a number of views are simultaneously visible, as exemplified in Figure 2(b). To the view originally intended to be visible with full brightness ("F" sub-pixels), views in the neighbouring zones seen with partial brightness are added, as denoted by "P". This effect can be regarded as *inter-channel crosstalk* [1], or *interperspective aliasing* [4].

When a 3D object is visualized on a multi-view display with n views, n different observations are interleaved into one compound 3D image. A flat 2D object, which is meant to appear floating in front or behind the screen surface, is represented by n identical observations. In this case, the optical filter can be regarded as a mask, which partially covers the underlying 2D image, or equivalently as a sub-sampling function applied to it. The slanted optical barrier introduces artefacts to the underlying image, which are modelled as aliasing. These artefacts are especially pronounced in flat, two-dimensional parts of the image. Graphical elements of the user interface, movie subtitles and 2D photographs are some examples of objects, prone to aliasing. Furthermore, aliasing artefacts are most pronounced for a static observer, since the group of visible pixels remains unchanged.

The effect of viewing simultaneously sub-pixels intended to be visible (those marked "F" in Figure 2(a)) with those, which belong to adjacent views (marked "P" in the same figure) has to been taken into account when modelling the sampling pattern. It is not a perfect binary mask but a more comprehensive masking function, where the visibility of each sub-pixel is affected by its relative position in respect to the optical filter.

Research on antialiasing filters for multi-view displays is rather scarce. Jain and Konrad [5] introduced a method for designing 2D non-separable antialiasing filters for an arbitrary sub-sampling pattern. They devised an optimization procedure targeting 2D filter with passband that spans all frequencies at which the contribution of all alias terms is smaller than the original signal itself. In [6], Moller and Travis used simplified optical filter model to analyse display bandwidth, and derive a spatially-varying 2D filter which requires knowledge of scene per-pixel depth. Zwicker *et al.*

[4] proposed a low-pass filter to be applied on the sampling grid of the multi-view display expressed in ray-space. Their approach aims at preventing both intra- and inter-perspective aliasing. However, their model assumes constant (i.e. vertical) masking pattern for each image row, which does not take into account the directionally dependant aliasing caused by slanted optical filter. In [7] the authors have proposed a methodology for designing optimal antialiasing filters, based on subjective preferences of the observer.

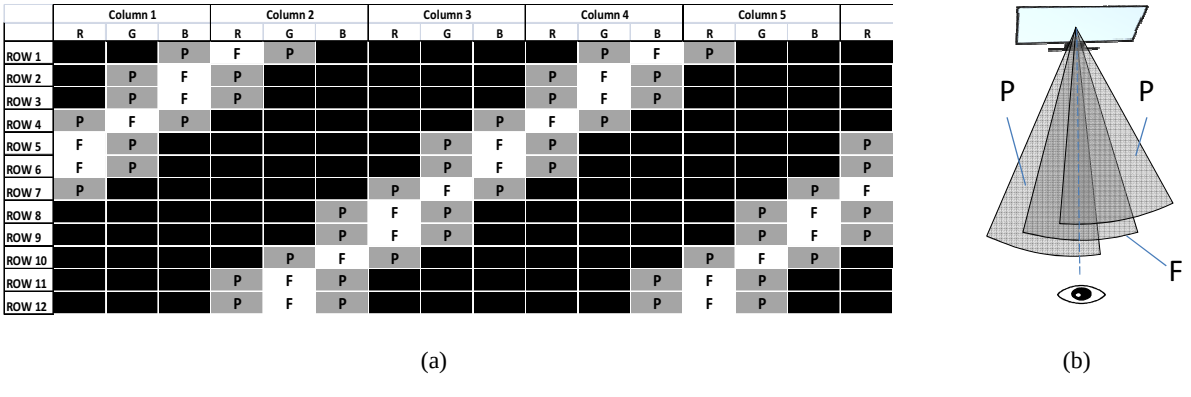

(a) (b)

Figure 2, Aliasing on multi-view displays: a) visibility of sub-pixels, b) interspersing of visibility zones

This paper presents an approach for designing optimal antialiasing filters based on objective criteria. Ideally, a precise model of the optical filter would allow optimal design. However, such model depends on optical parameters of the display which are rarely provided to the owner. An alternative approach, described in this paper, is to directly measure the relevant optical properties of a multi-view display, and use the measurement results for designing the optimal antialiasing filter.

The paper is organized as follows: Section 2 gives insights about the way optical parameters of a multi-view display can be estimated, and presents measurement results for a particular multi-view display, regarded as a case study. In Section 3, two different methodologies for designing antialiasing filters optimized for a specific 3D display are presented. First, the measurement results are used for creating a model and designing non-separable 2D antialiasing filter for the considered display. Then, an attempt is done to reproduce comparable results using less-computationally demanding separable filters. Section 4 presents objective results based on numerical comparison, as well as subjective results for visual inspection.

2. MEASUREMENT OF DISPLAY PROPERTIES

A multi-view autostereoscopic display is a nonlinear system that transforms, depending on the observation angle, a digital image into several, somehow distinct, images or views. As described in the previous section, this is achieved by the display architecture i.e. LCD matrix combined with an optical filter. An observer staying within one view (looking at the display from a particular direction) will see only a fraction of the original image, that is, he/she will see a downsampled version of the image. In order to represent the image correctly and foremost to avoid alias errors caused by downsampling it is necessary to filter the image with an antialiasing filter before it is sent to the display. The design of the antialiasing filter requires the knowledge about the frequency properties of the display. A detailed procedure for measuring various properties of autostereoscopic displays is given in [9]. For convenience of the reader, some material from [9] is given in this section with the emphasis put on the frequency properties of the display.

2.1 Sub-pixel visibility versus observation angle

The optical filter of a multi-view display is directionally selective. The apparent brightness of each pixel depends on its intensity, its position in respect to the optical filter, and the position of the observer (distance and observation angle) in respect to the display. The brightness of a sub-pixel can be measured by photographing the display at various angles. In this work, the effect of the optical filter is modelled as *visibility* of each sub-pixel. Visibility of a sub-pixel is the ratio between the assigned intensity and the measured brightness of that pixel. For gamma corrected and normalized images, visibility is a scaling coefficient between 0 and 1. It is assumed, that all sub-pixels, which belong to one view are equally affected by the optical filter, and have maximum visibility for the optimal observation spot of that view. The visibility of each sub-pixel as a function of the observation angle is measured by the following general measurement methodology of five steps. As a case study, this paper presents measurement results for 23" 3D Display AD built by X3D-Technologies GmbH, which is hereafter referred to as *X3D display*. Further details about the measurements can be found in [8] and [9].

The first step is to derive the size of interleaving pattern by observing the behavior of various test patterns. Such test pattern is an image where every *n*-th sub-pixel in a row and every *m*-th sub-pixel in a column are fully lit, and the rest are black. The test pattern with the correct size is fully invisible for most observation angles. The interleaving pattern of X3D display is found to be 8 sub-pixels wide and 12 rows high. The next step is to prepare a group of test images, where only one sub-pixel per pattern with that size is lit, and to find the optimal observation spot of each group. The sub-pixels which have the same optimal observation spot belong to a single view. The views are numbered by order of appearance of their optimal observation spot. For X3D display there are 24 such groups, which results in an interleaving pattern as shown in Figure 3(a). Finally, test images are generated where only sub-pixels belonging to one view are fully lit. The brightness of each test image is measured from each optimal observation spot. The mean brightness measured on an area of the screen gives the visibility of the sub-pixels, which belong to the same view, as seen from the chosen observation spot. For X3D display, the brightness of each view as seen in front of the centre of the display is given in Figure 3(b). The measurements for other observation spots produce similar curves, with peaks (maximum visibility) shifted to the corresponding view.

	Column 1			Column 2			Column 3			Column 4			Column 5			
	R	G	B	R	G	B	R	G	B	R	G	B	R	G	B	R
ROW 1	2	5	8	11	14	17	20	23	2	5	8	11	14	17	20	23
ROW 2	4	7	10	13	16	19	22	1	4	7	10	13	16	19	22	1
ROW 3	6	9	12	15	18	21	24	3	6	9	12	15	18	21	24	3
ROW 4	8	11	14	17	20	23	2	5	8	11	14	17	20	23	2	5
ROW 5	10	13	16	19	22	1	4	7	10	13	16	19	22	1	4	7
ROW 6	12	15	18	21	24	3	6	9	12	15	18	21	24	3	6	9
ROW 7	14	17	20	23	2	5	8	11	14	17	20	23	2	5	8	11
ROW 8	16	19	22	1	4	7	10	13	16	19	22	1	4	7	10	13
ROW 9	18	21	24	3	6	9	12	15	18	21	24	3	6	9	12	15
ROW 10	20	23	2	5	8	11	14	17	20	23	2	5	8	11	14	17
ROW 11	22	1	4	7	10	13	16	19	22	1	4	7	10	13	16	19
ROW 12	24	3	6	9	12	15	18	21	24	3	6	9	12	15	18	21

(a)

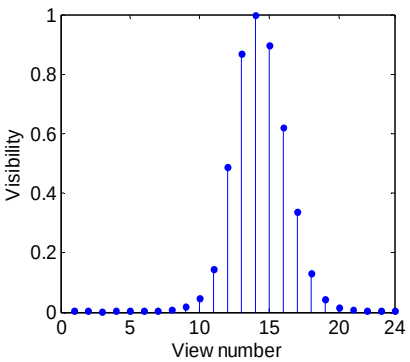

(b)

Figure 3, Measurement results a) derived interleaving pattern of X3D display, b) sub-pixel visibility versus view number, from the optimal observation spot of view 14

2.2 Frequency response of multi-view displays

An elegant way for deriving the frequency response of the display, especially when not all display specifications are available, is by using measurements. The main idea in this approach is to generate a set of test images containing signals with various known frequencies, visualize them on the display, and then analyze the output of the display. This procedure is described in the following three subsections. Whereas the approach is illustrated for the X3D display, it is perfectly applicable for any other multiview displays.

2.2.1 Test images

For the purpose of measuring the frequency response of the display, numerous test images (hereafter referred to as input images) have been generated. Each of them is a pattern of a known frequency. Two of those images for frequencies[1] (f_x, f_y) = (0.2, 0) and (f_x, f_y) = (0.2, –0.3) are shown in Figure 4 with the corresponding spectra shown in Figure 5. Here, f_x and f_y refer to frequencies along the x and y axis, respectively. The idea behind generating these images lies in the fact that their frequency behaviour is well known, that is, they have well defined, known, distinct frequency components as it can be seen in Figure 5. In both cases, in Figure 5, the central peak at (f_x, f_y) = (0, 0) is the DC component and should be ignored.

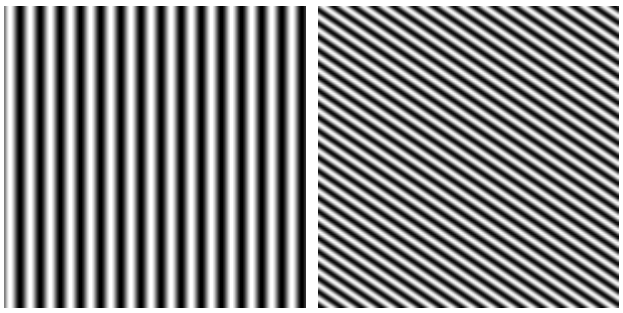

(a) (b)

Figure 4, Example of input (test) images. (a) (f_x, f_y) = (0.2, 0). (b) (f_x, f_y) = (0.2, –0.3).

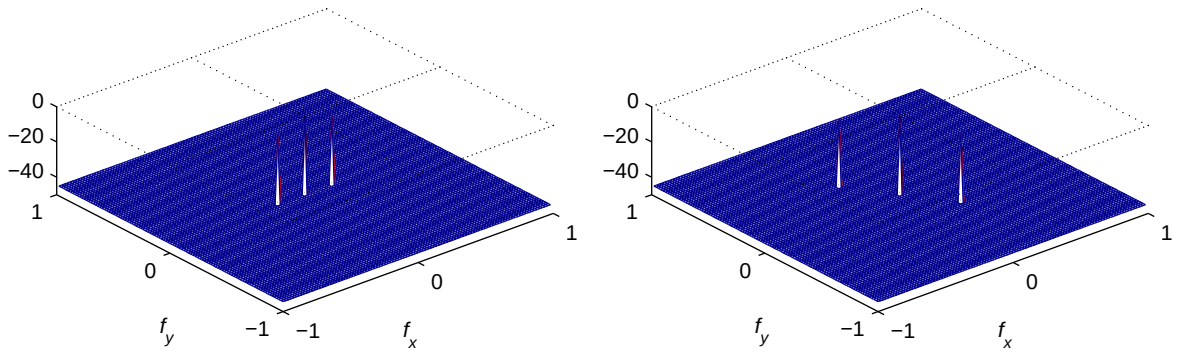

(a) (b)

Figure 5, Example of input images – Spectra. (a) (f_x, f_y) = (0.2, 0). (b) (f_x, f_y) = (0.2, –0.3).

Several hundreds of those images were generated for sets of frequencies f_x and f_y belonging to the intervals $f_x \in [0, 1]$ and $f_y \in [–1, 1]$ (the signals for $f_x \in [–1, 0)$ and $f_y \in [–1, 1]$ can be easily reconstructed by taking into account symmetry

[1] In this paper all frequencies are normalized to $f_s/2=1$ with f_s being the sampling frequency.

properties of spectra of real signals). By selecting, on the above intervals, a dense grid of frequencies (e.g. $\Delta_f \geq 0.01$), all possible combinations for input images are taken into consideration. It should be pointed out that a denser grid results in a more precise estimation (better resolution) of the frequency response but it also considerably increases the number of required measurements. Therefore, a proper compromise between the required resolution and the number of measurements has to be made. In this paper the step $\Delta_f = 0.025$ has been used. This has turned out to be a good choice for designing antialiasing filters for the display under consideration.

2.2.2 Measurements

The input images, described in the previous section, have been visualized on the display and, by using a high resolution digital camera, photos of the screen have been taken (hereafter referred to as output images). As an example, for the input images shown in Figure 4 the output images are given in Figure 6 (images have been enhanced for clarity). The spectra of these images are shown in Figure 7.

Three observations can be made based on these measurements. First, although each of the input images contains only a single frequency component, the output images contain numerous different frequency components. This is mainly due to the aliasing and imaging effects of the display. As already discussed before, aliasing is the consequence of having multiple views, that is, from one observation angle only part of pixels is visible. This corresponds to downsampling of the original image. Aliasing effects can be removed by a proper antialiasing filter. On the other hand, imaging occurs due to the gaps between visible sub-pixels (See Figure 3(a)). In the spectral domain, imaging can be seen as high frequency components. Unfortunately imaging cannot be avoided or compensated by any filtering as it occurs in the display. Fortunately, as long as no aliasing occurs, it has been experimentally shown that those imaging components are partially suppressed by human visual system (e.g in Figure 6(a) the vertically lines are still seen even if they are heavily broken).

Second, if the frequency of the signal is low, then the signals can be correctly represented on the display (e.g. it is easy to identify vertical lines in Figure 6(a)). However, if the signal frequency is too high then due to the aliasing and imaging effects the image on the display would differ from the original one (e.g. in Figure 6(b), beside the barely visible diagonal lines from Figure 4(b) many other lines are also seen).

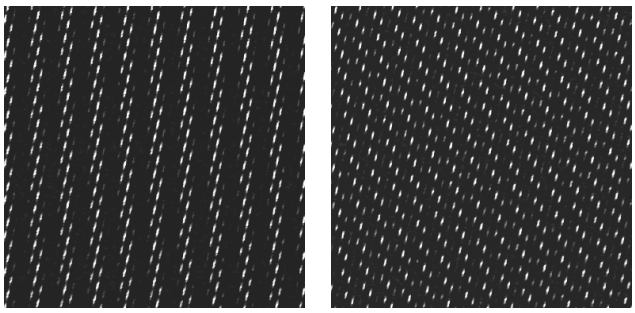

(a) (b)

Figure 6, Example of output images (photos taken from the display). (a) $(f_x, f_y) = (0.2, 0)$. (b) $(f_x, f_y) = (0.2, -0.3)$.

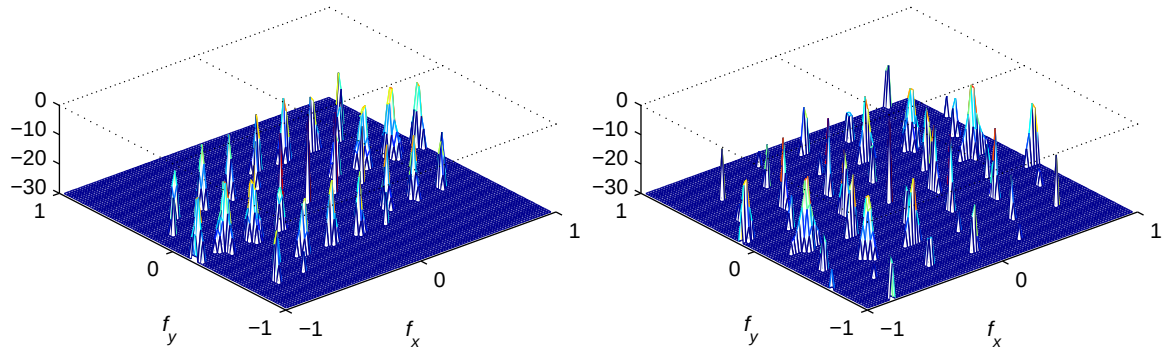

(a) (b)

Figure 7, Example of output images – Spectra. (a) (f_x, f_y) = (0.2, 0). (b) (f_x, f_y) = (0.2, –0.3).

Third, the monitor introduces nonlinear distortions as illustrated by Figure 8. Figure 8(a) and Figure 8(b) show the spectra along the *x*-axis for the input signal (f_x, f_y) = (0.2, 0) and the corresponding output signal, respectively. Although the input signal has only one spectral component (at f_x = 0.2), the output signal also contains some higher harmonics (at f_x = 0.4) approximately 6-8 dB lower than the main spectral component.

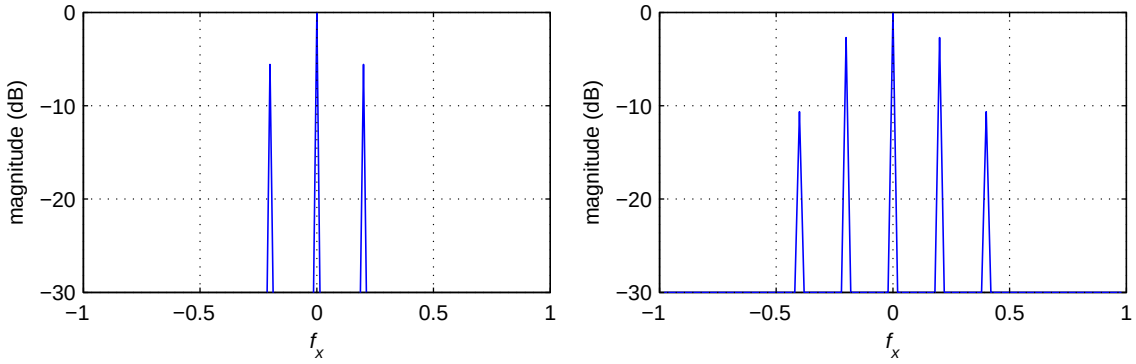

(a) (b)

Figure 8, Nonlinear distortions – Spectra along *x*-axis for signal (f_x, f_y) = (0.2, 0). (a) Input image. (b) Output image.

2.2.3 Frequency characteristics of the ideal antialiasing filter

In order to analyze the performance of the display in the frequency domain, the spectra of the input and output images derived in the previous two sections were compared. In order to eliminate measurement errors (noise) the spectrum of the output image has been thresholded to -30dB below the strongest frequency component.

The criteria for determining if a given frequency component passes through the system properly or it is distorted by aliasing and imaging errors was the following: For every input signal of frequency $(f_{x_0},\ f_{y_0})$ it was checked if the contributing aliasing / imaging components contain frequency components that are inside a circle with radius

$$r_0 = \sqrt{f_{x_0}^2 + f_{y_0}^2}\ ,$$

that is, if they are of a smaller frequency than the original one (in all cases the DC component is ignored). If there are frequency components smaller than the one present in the input signals, this means that the system aliased some of the frequencies and as a consequence, there will be visible distortions on the display. By removing such frequencies from

the input image, aliasing effects can be avoided. Hence, the stopband of the antialiasing filter should suppress all those frequencies.

Two examples of spectra (represented as contour plots) of output images are shown in Figure 9. This corresponds to the two examples used in the previous sections. Figure 9(a) and Figure 9(b) are magnified (contour) version of figures Figure 7(a) and Figure 7(b), respectively. In these figures only the part containing frequencies smaller than r_0 (represented by the red circle) is shown. As seen from the figures, in the first example, there are no spectral components that are of a lower frequency than the one used for generating the input image and therefore the image is properly represented on the display. In the second example, the output image considerably differs from the one sent to the display due to the aliasing errors. In the spectral domain this can be noticed by presence of several frequency components that are inside the circle with radius r_0. There is no point in trying to represent this image on the display under consideration, that is, this frequency should be suppressed before visualizing the image on the display.

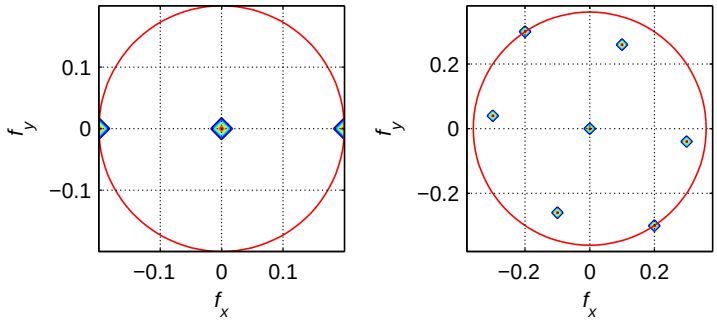

(a) (b)

Figure 9, Spectra of output images. (a) (f_{x0}, f_{y0}) = (0.2, 0), r_0=0.2. (b) (f_{x0}, f_{y0}) = (0.2, – 0.3), r_0=0.36.

By applying the above criteria to all output images, the passband (frequencies that do not cause aliasing) and stopband (frequencies that do cause aliasing) can be classified as given in Figure 10(a). In this figure, the passband is represented by dots. In order to get a smoother filter characteristic that can be used in the filter design, a 5 by 5 median filter has been applied resulting in the desired ideal cut-off frequency of an antialiasing filter shown in Figure 10(b). Such ideal filter would suppress all undesired frequency components in the image resulting in an alias-free image.

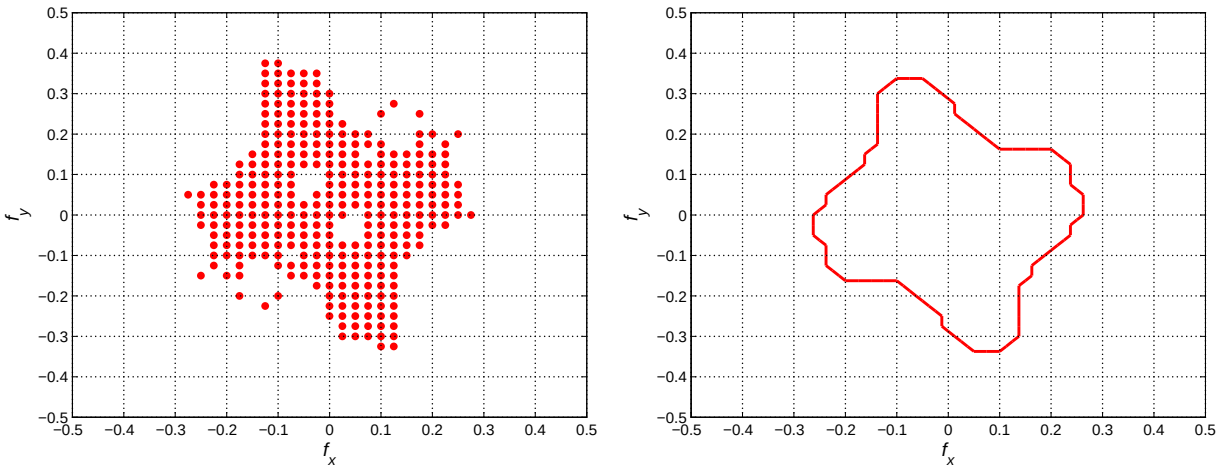

(a) (b)

Figure 10, Ideal 2D filter. (a) Passband region estimation based on measurements. (b) Contour of the ideal filter.

3. DESIGN OF ANTIALIASING FILTERS

The discussion in previous sections argued why it is important to filter an image before visualizing it on an autostereoscopic display. In an earlier paper [7], it has been shown that visually good results can be achieved with separable 2D antialiasing filters that were optimized by subjective experiments. However, in practice it is better to have an objective design method that does not depend on subjective testing. Therefore, based on the results of the measurements described in the previous sections, in the following two sections separable and non-separable 2D filters are designed for the display under consideration.

3.1 Non-separable antialiasing filters

For the display under consideration, the shape of an ideal 2D antialiasing filter is shown in Figure 10(b). In this figure, the curve shows the ideal cut-off frequency, that is, the passband of the filter should be inside the contour, and its stopband everywhere else. For designing a non-separable 2D filter approximating this ideal one, the windowing design technique with the Kaiser window of length 24 has been used (e.g. see `fwind2` function in Matlab) [10]. The design results in the 24 by 24 2D non-separable filter with impulse response shown in Figure 11(a). The corresponding magnitude response (contour) of the designed filter is shown in Figure 11(b). The Kaiser window has been selected as a good candidate due to its narrow transition band and flexible attenuation. The variable parameter of the Kaiser window controlling the stopband attenuation has been set to β=2.2. Such selection will ensure a stopband attenuation of at least 30dB that is good enough for the display under consideration.

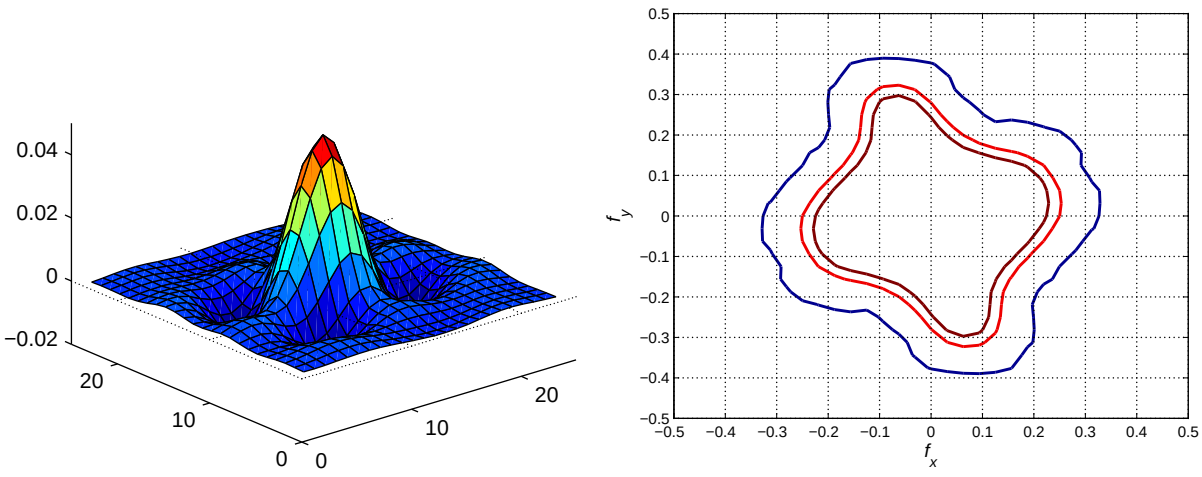

(a) (b)

Figure 11, 2D non-separable filter. (a) Impulse response. (b) Magnitude response – contour for -3 (innermost line), -6, and -30 dB (outermost line).

The -6dB line in Figure 11(b) approximates the ideal cut-off frequency. Due to the finite transition bandwidth of the designed filter, even after applying it to the input image, some aliasing errors will occur on the display. However the aliased frequencies will be attenuated by the filter (either filter transition band or stopband) and as such they will not be visible. A sharper filter can be generated by increasing the filter order, which in turn, increases the number of multiplication required for filtering the image. On the other hand, filters of a smaller size will approximate the edge of

the ideal filter with lower precision. Moreover, sharper filters have also a tendency to cause edge artifacts in filtered images. Therefore, filter size of 24 by 24 has been chosen as a good compromise between the implementation complexity, transition bandwidth, and approximation of the ideal filter.

3.2 Separable filters

The 2D non-separable filter proposed in the previous section is a very good approximation of the ideal one given by Figure 10(b). However, the computational complexity of a 2D filter is rather high. Considerable computational savings are achieved if the 2D filter can be separated into two 1D filters, one filtering in the horizontal direction and one in the vertical direction. As long as similar performances are achieved by separable and non-separable filters, for a similar filter size, the separable filters will be considerably faster.

For deriving a separable 2D antialiasing filter, the 24-view model described in Section 2.1 is utilized. Based on this model, a pattern of visible pixels that can be seen from one observation point has been derived as seen in Figure 3. The Spectrum of this pattern is shown in Figure 12. Due to downsampling/upsampling behaviour of the display, each of the peaks in this spectrum corresponds to a source of aliasing. In order to avoid aliasing, a filter has to be designed in such a way that its passband does not overlap with any of its copies generated by moving its centre to any of those aliasing sources.

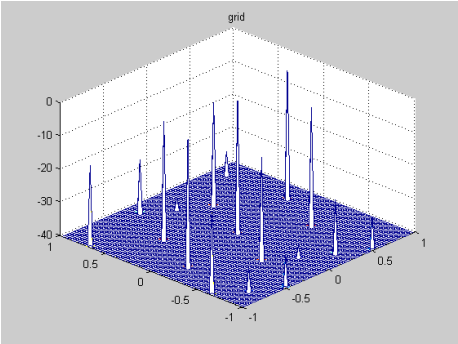

Figure 12, Spectrum of sub-sampling pattern for one view based on the 24-view model.

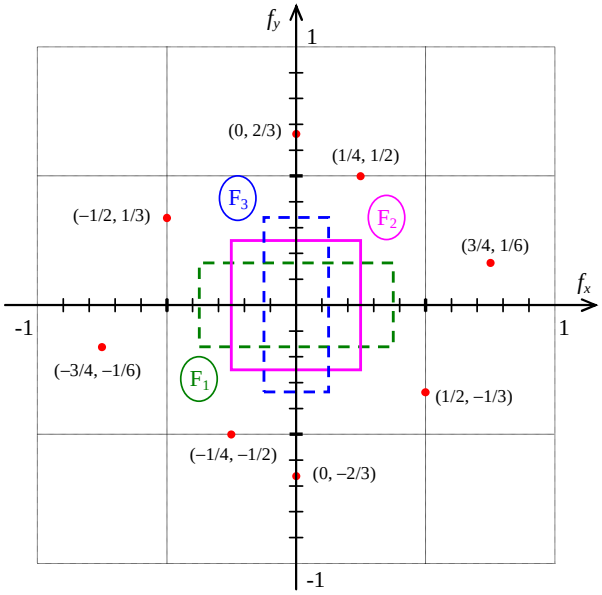

Figure 13, Various ideal separable antialiasing filters.

Additional restriction when using separable filters is that only rectangular-shaped 2D filters can be designed that are symmetrical along the *x* and *y* axis. By following basic downsampling principles, it is obvious that there are several different separable filters that can be used as antialiasing filters for this display. This is illustrated in Figure 13. In this figure centres of aliasing terms are marked by red dots with the exact coordinates (frequencies) of each component given in parenthesis as (f_x, f_y) pairs. Moreover only the aliasing terms from Figure 12 pertinent for the design of antialiasing filters are shown. In the figure, three possible ideal filters are drawn (marked as F_1, F_2 and F_3). Each of those filters will perform proper antialiasing, but due to different shapes the visual quality of displayed images will be different. The numerical data for these filters is given in Table I. In the table, f_{cx} and f_{cy} stand for the ideal filter cut-off frequencies in horizontal and vertical direction, respectively.

Table I Horizontal (f_{cx}) and vertical (f_{cy}) cut-off frequencies for ideal separable antialiasing filters

Filter	F_1	F_2	F_3
f_{cx}	3/8	1/4	1/8
f_{cy}	1/6	1/4	1/3

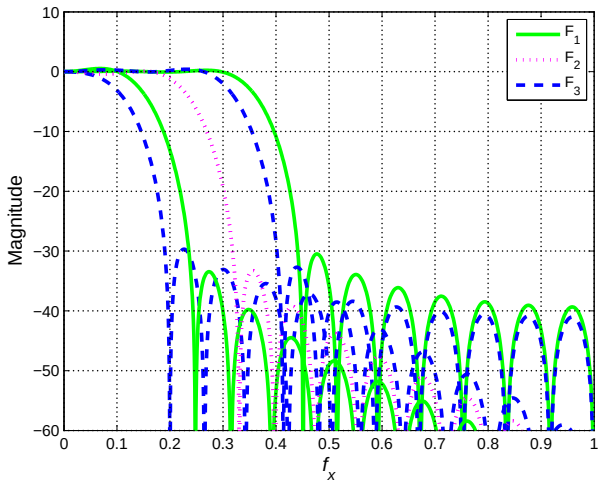

Figure 14, Various ideal, horizontal (solid line) and vertical (dashed line), antialiasing filters of order $N = 23$ for F_1 (green, solid line), F_2 (magenta, dotted line), and F_3 (blue, dashed line). The horizontal and vertical components of F_2 overlap.

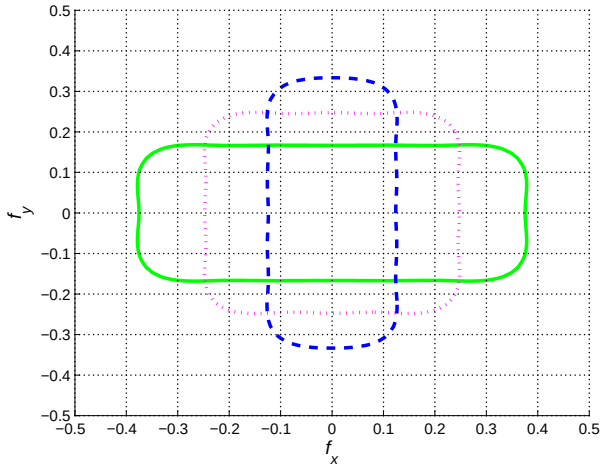

Figure 15, Magnitude responses: – 6dB contour for F_1 (green, solid line), F_2 (magenta, dotted line), and F_3 (blue, dashed line).

For designing 1D filters with cut-off frequencies given in Table I, as in the case of non-separable design, the windowing technique with the Kaiser window of length 24 has been used. The variable parameter of the Kaiser window has been set to $\beta = 2.2$. The magnitude responses of the designed filters are given in Figure 14. Solid and dashed lines represent the horizontal and vertical filters, respectively. The magnitude responses (contour) of the corresponding 2D filters are given in Figure 15.

4. RESULTS

In this section, the advantage of the proposed methodology with respect to previously suggested antialiasing filter design approaches is demonstrated by objective comparisons of filter performance and computational efficiency and by visual inspection on a set of test images.

4.1 Numerical comparison between filters

The passband size was evaluated as the passband area of the 2D filter or in the case of separable filter, passband area of the corresponding 2D filter, shown in Figure 15. The implementation complexity is given as the number of multiplications per pixel and is denoted by *C*. The results of both comparisons are given in Table II. Moreover, for completeness of the results, the filters designed in this paper are also compared with the ones presented in [7]. In that work two filters have been suggested, denoted as 'smooth' ad 'sharp' due to their effect on the processed image. The 'smooth' one was aimed at total alias terms suppression while the 'sharp' one was optimized visually to allow for some small amount o aliasing for the sake of better sharpness.

Table II Numerical comparison of various antialiasing filters

	Proposed in this work				Presented in [7]		
Filter	2D	F_1	F_2	F_3	JK	'smooth'	'sharp'
size (length)	24 by 24	24	24	24	48 by 48	15, 18	23, 23
Passband area	.048	0.063	0.063	0.042	0.068	0.033	0.107
C	576	48	48	48	2304	33	46

Several observations can be made based on Table II. First, it is obvious that non-separable filters require considerable higher number of multiplications than the separable ones. Furthermore, the separable filters proposed in this paper are of higher order than the ones denoted as 'smooth' in [7]. This was caused mainly by attempting to widen the passband (e.g. in filter F_2). A wider passband suppress less amount of frequencies in the information part of the signal. However, it imposes also a narrower transition band, and thus a higher filter order, so to ensure effective alias suppression around the passband edge.

Second, when comparing the proposed 2D filters and the one designed by the Jain and Konrad [1], it can be seen that the passband area of the proposed filters is smaller. This is due to the nonlinear distortions (see Section 2.2.2) that exist in the display but are not taken into account by the model used by Jain and Konrad. Moreover, because of these distortions, the filters used in [1] had to be of a higher order to provide shorter transition bandwidths thereby eliminating the alias components caused by the nonlinear distortions.

Third, from the three 1D filters (F_1, F_2 and F_3) proposed in previous section, F_2 has the best approximation of the ideal shape given by Figure 10(b). It will be demonstrated in Section 4.2 that it also performs best in visual inspections.

Forth, when using separable filters some minor aliasing errors are to be expected, because with separable filters it is impossible to get the ideal 2D shape shown in Figure 10(b). Nevertheless, it can be claimed, based on numerous experiments, that this aliasing is tolerable and does not compromise the image quality.

Fifth, the complexity evaluation in the table assumes direct implementation of every filter because in this way it is easy to have a relative comparison between filters. If in the implementation the coefficient symmetry is utilized and/or some other algorithms for fast implementation of a filter are used then the implementation complexity, for all filters in the table, can be further reduced.

4.2 Visual inspection

The performance of different antialiasing filtering is illustrated by presenting the filtering effect on three test images. Each image has been filtered with the set of filters, visualized on X3D display and then photographed.

The first image, denoted as 'Patterns' contains straight lines and patterns with high contrast and varying spatial frequencies. As a use case, it represents 2D geometric content found in a graphical user interface and it is particularly suitable for demonstrating aliasing effects. For example, the slanted lines in the image are at angles, which are most affected by the optical filter of the X3D display. The original test image is presented in Figure 16(a). The same image photographed as visualized on X3D display is shown in Figure 16(b). Structural and colour artefacts due to aliasing are clearly visible. Photographs of the test image, pre-processed with two different filters are given in Figure 16 (c) and (d). Figure 16(c) shows the image as pre-filtered by 2D non separable filter. Figure 16 (d) shows the image as pre-filtered by separable filter F_2. One can see that the image filtered by the non-separable filter exhibits no aliasing artefacts, while the image filtered by F_2 preserves more details, but some elements are still aliased.

The second test image consists of 2D text with variable font size, created by Wordle [11]. The original test image is given in Figure 17(a). The images in Figure 17 (b), (c) and (d) are photographs of the test image, pre-filtered by 2D filter, F_1 and F_2 respectively. Visual inspection shows that 2D filter and F_2 produce comparable results in terms of perceptual quality. Even though filters F_1 and F_2 have equal size of the passband area, images filtered by F_2 are easier to read due to the fact that F_2 has the same throughput in horizontal and vertical direction.

Finally, the filters are visually compared using full-colour, natural 2D image. The image is "Lighthouse" from the Kodak Image Database [12]. The results produced by the non-separable and separable (F_2) filters are quite similar for that image. One can conclude that for natural images containing low or no amount of slanted patterns at 'critical' angles (determined by the topology of the optical filter slant) the performance of the F_2 filter is quite competitive to that of the non-separable filter being closest to the ideal antialiasing filter for the given sampling topology.

5. CONCLUSIONS

In this article, we have proposed a methodology for designing antialiasing filters for autostereoscopic displays. Such displays are characterized by additional optical layer (filter) on top of conventional LCD to create different views for different directions. The attempt to create a number of different views reduces the spatial resolution and in order to cope with this problem, the optical layer is mounted in a slanted manner. While this design offers a good compromise between spatial resolution and number of views, it also specifies a more complex non-rectangular sub-sampling pattern on a sub-pixel level. Our methodology is based on simple, yet precise enough measurements of the aliasing effects on the display. Only basic knowledge about the display, e.g. resolution is required to design and conduct the measurements. This is in contrast with previous approaches proposed in the literature which require more detailed

knowledge about the construction of the displays. Other previous approaches suggested modelling (and sometimes simplifying) the view sub-sampling topology. Such models however cannot predict possible nonlinearity in the optical system which is also source of aliasing artefacts. However, it is well revealed by our measurement methodology and subsequently taken into account in the filter design.

The form of the measured passband is such that requires a 2D non-separable filter with certain order. While designing such a filter, alternatively we have designed also a separable approximation which competed favourably in terms of visual performance and computational cost. The design is fairly automatic and little interaction with the user is required (e.g. selection of filter orders). The design is robust to variations of the input parameters so even a not so precise choice by the user will lead to satisfactory results.

We have considered the case where images are placed at the screen surface (images for the left and right eye having zero disparity). Our future work will consider the case of changing disparity and its influence on the antialiasing filtering.

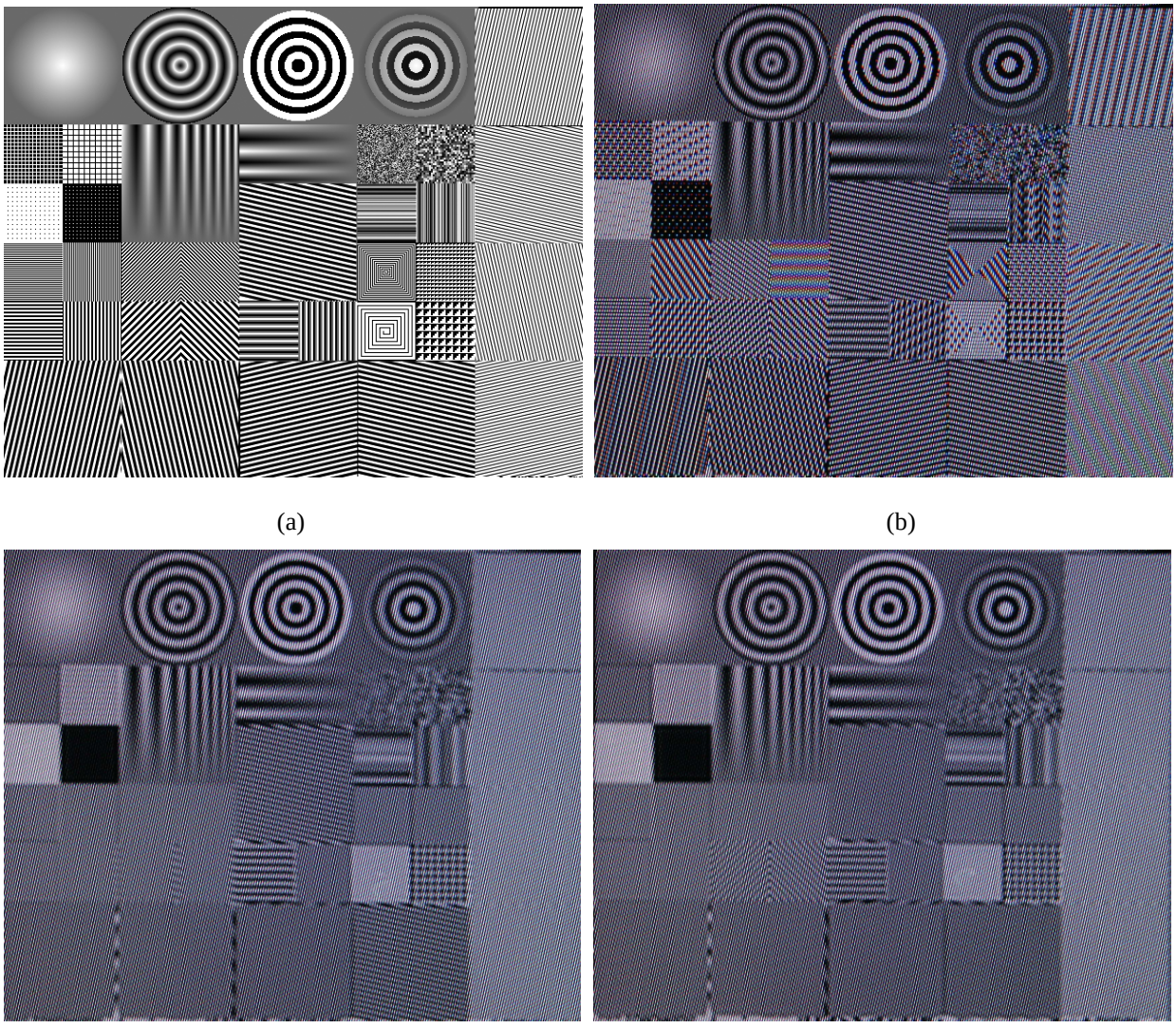

(a) (b)

(c) (d)

Figure 16, Test image with geometric lines: a) original image, (b-d) images, photographed on X3D display, as follows – b) unprocessed image, exhibiting aliasing, c) filtered with 2D filter, d), filtered with F_2.

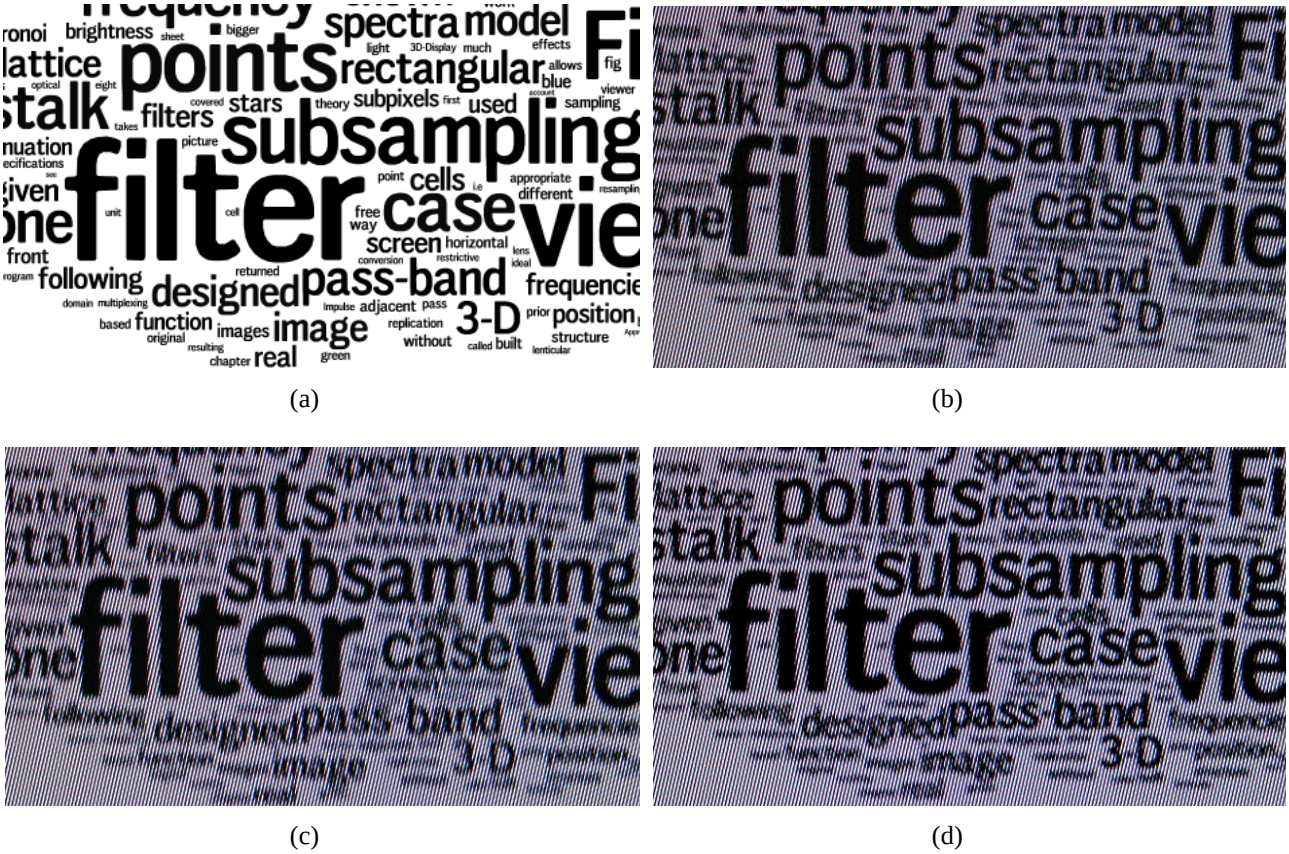

Figure 17, Test image with text: a) original image, (b-d) images, pre-filtered and photographed on X3D display, as follows – b) pre-filtered with 2D filter, c) pre-filtered with F_1, d) pre-filtered with F_2. Note: unprocessed image with aliased text is clearly with the worst quality, but is not shown here because of space limitations.

(a) **(b)**

(c) **(d)**

Figure 18, 2D full-colour test image: a) original image, (b-d) images, photographed on X3D display, as follows – b) unprocessed image, exhibiting crosstalk, c) pre-filtered with 2D filter, d) pre-filtered with F_2.

REFERENCES

[1] C. Van Berkel and J. Clarke, “Characterisation and optimisation of 3D-LCD module design”, in Proc. SPIE Vol. 2653, Stereoscopic Displays and Virtual Reality Systems IV, (Fisher, Merritt, Bolas, edts.), pp. 179-186, May 1997

[2] S. Pastoor, “3D displays”, in (Schreer, Kauff, Sikora, edts.) 3D Video Communication, Wiley, 2005.

[3] A. Schmidt and A. Grasnick, "Multi-viewpoint autostereoscopic displays from 4D-vision", in Proc. SPIE Photonics West 2002: Electronic Imaging, vol. 4660, pp. 212-221, 2002

[4] Zwicker, M., Matusik, W., Durand, F., Pfister, H., and Forlines, C. 2006. Antialiasing for automultiscopic 3D displays. In *ACM SIGGRAPH 2006 Sketches* (Boston, Massachusetts, July 30 - August 03, 2006). SIGGRAPH '06. ACM, New York, NY, 107.

[5] A. Jain and J. Konrad, “Crosstalk on automultiscopic 3-D displays: Blessing in disguise?,” in Proc IS&T/SPIE Symposium on Electronic Imaging, Stereoscopic Displays and Applications, San Jose, CA, Vol. 6490, pp. 649012 (2007).

[6] Moller, C. N. and Travis, A. R. 2005. Correcting Interperspective Aliasing in Autostereoscopic Displays. *IEEE Transactions on Visualization and Computer Graphics* 11, 2 (Mar. 2005), 228-236.

[7] A. Boev, R. Bregovic, A. Gotchev, K. Egiazarian, Anti-aliasing filtering of 2D images for multi-view auto-stereoscopic displays, in Proc. of *The 2009 International Workshop on Local and Non-Local Approximation in Image Processing, LNLA 2009*, Helsinki, Finland, 2009

[8] A. Boev, A. Gotchev and K. Egiazarian, “Crosstalk measurement methodology for auto-stereoscopic screens”, Proc. of 3DTV Con, Kos, Greece, 2007

[9] A. Boev, R. Bregovic, A. Gotchev, “Measuring and modeling per-element angular visibility in multiview displays”, *Special issue on 3D displays, Journal of Society for Information Display*, to be published

[10] S. K. Mitra, Digital signal processing: A computer based approach, New York: McGrow-Hill, 2005

[11] Wordle, software for generating “word clouds”, available online at http://www.wordle.net

[12] Kodak image database, available online at ftp://ftp.kodak.com/www/images/pcd